Available online at www.sciencedirect.com

ScienceDirect

Geochimica et Cosmochimica Acta 151 (2015) 34–48

Geochimica et Cosmochimica Acta

www.elsevier.com/locate/gca

A kinetic pressure effect on the experimental abiotic reduction of aqueous CO_2 to methane from 1 to 3.5 kbar at 300 °C

Codi Lazar [a,*], George D. Cody [a], Jeffrey M. Davis [b]

[a] Geophysical Laboratory, Carnegie Institution of Washington, 5251 Broad Branch Road NW, Washington, DC 20015, USA
[b] National Institute of Standards and Technology, Surface and Microanalysis Science Microanalysis Research Group, Gaithersburg, MD 20899, USA

Received 29 July 2013; accepted in revised form 15 November 2014; Available online 22 November 2014

Abstract

Aqueous abiotic methane concentrations in a range of geologic settings are below levels expected for equilibrium with coexisting CO_2 and H_2, indicating that kinetics can control the speciation of reduced carbon-bearing fluids. Previous studies have suggested that mineral catalysts or gas-phase reactions may increase the rate of methanogenesis. Here, we report on experiments that indicate pressure can also accelerate aqueous reduction of CO_2 to CH_4. Four series of cold-seal hydrothermal experiments were performed from 1 to 3.5 kbar at 300 °C for two weeks and analyzed using gas chromatography/mass spectrometry. The starting fluids were 10–20-μL solutions of 70-mmolal ^{13}C-labeled formic acid ($H^{13}COOH$) contained in welded gold capsules. Increasing pressure (P) resulted in a systematic, reproducible log-linear increase in $^{13}CH_4$ yields. The pressure effect could be quantified the log-linear slope, $\Delta\log[^{13}CH_4]/\Delta P$ (log mmolal per kbar). The mean slope was 0.66 ± 0.05 ($\pm$1s.e.), indicating that $^{13}CH_4$ yields increased by an average factor of 40–50 over a P range of 2.5 kbar. Pressure-independent variations in $[^{13}CH_4]$ were observed as scatter about the log-linear regressions and as variations in the y-intercepts of the regressions. These variations were attributed to trace amounts of catalytic Fe along the inner capsule wall that remained despite cleaning the Au capsules in nitric acid prior to each experimental series. The mechanism for the pressure-dependent effect was interpreted to result from one or more of the following three processes: reduction of a metastable reaction intermediate such as methanol, formation of Fe-carbonyl complexes in the fluid, and/or heterogeneous catalysis by Fe. The results suggest that pressure may influence aqueous abiotic CH_4 yields in certain geological environments, particularly when the relative effects of other kinetic factors such as temperature are diminished, e.g., in cool forearcs or other settings with a steep geothermal gradient. Because the experiments were performed over a limited pressure range, even modest isothermal increases in pressure may substantially enhance CH_4 yields. A kinetic pressure effect may be especially important on the deep ocean floors of planetary bodies where pressure may compensate for the otherwise sluggish reaction kinetics expected at low T.
© 2014 Elsevier Ltd. All rights reserved.

1. INTRODUCTION

Aqueous abiotic methane formed during water–rock interaction has been ascribed astrobiological significance as a nutrient for lithoautotrophic microbial communities (Kelley et al., 2005; Proskurowski et al., 2008), a greenhouse gas on the early Earth (Kasting, 2005), an alternative to microbial methane in the Martian atmosphere (Lyons et al., 2005), and a precursor to prebiotic compounds (Miller and Urey, 1959). Methane may also polymerize to form heavier alkanes (Horita and Berndt, 1999), although the global inventory of abiotic hydrocarbons is minor relative to thermogenic deposits (Sherwood-Lollar et al., 2002). Many aqueous geological environments satisfy the

* Corresponding author.
E-mail address: clazar@carnegiescience.edu (C. Lazar).

http://dx.doi.org/10.1016/j.gca.2014.11.010
0016-7037/© 2014 Elsevier Ltd. All rights reserved.

thermodynamic criteria for CH_4 stability in C–O–H fluids, and abiotic methane has been proposed to exist in basaltic and ultramafic hydrothermal systems along mid-ocean ridges (Ingmanson and Dowler, 1977; Kelley, 1996; Charlou et al., 1998, 2002; Proskurowski et al., 2008), groundwaters of Precambrian crystalline basements (Sherwood-Lollar et al., 2002), graphite-saturated metamorphic settings (French, 1966), continental fumaroles (Fiebig et al., 2007), fluid inclusions in continental alkaline igneous rocks (Potter et al., 2004), and forearc serpentine mud volcanoes (Mottl et al., 2003).

Aqueous abiotic methanogenesis is a sluggish process at hydrothermal conditions. Methane concentrations in natural and experimental hydrothermal systems are commonly below those predicted from equilibrium with coexisting CO_2 and H_2 (Janecky and Seyfried, 1986; Shock, 1988, 1990; Charlou et al., 1998, 2000; McCollom and Seewald, 2001), indicating that kinetics may control fluid compositions. Influenced by well-established industrial techniques such as the Fischer–Tropsch (Fischer and Tropsch, 1926; Roferdepoorter, 1981) and Sabatier (Sabatier and Gaudion, 1919; Brooks et al., 2007) processes, much geochemical research on the kinetics of natural aqueous methanogenesis has focused on heterogeneous catalysis by transition metal accessory minerals such as Ni–Fe alloy (Horita and Berndt, 1999), Fe-chromite (Foustoukos and Seyfried, 2004), pure Fe° metal (McCollom and Seewald, 2006), Ni–sulfides (Fu et al., 2008), cobalt-bearing magnetite (Co:Fe = 1:3) (Ji et al., 2008), and magnetite (Fu et al., 2007). Temperature (T) must play a role, and it has also been suggested that reaction in a gas phase may also accelerate methanogenesis (McCollom and Seewald, 2001).

Another potentially important kinetic variable in aqueous methanogenesis is pressure, which has been previously observed to enhance reaction yields in a variety of more complex organic reactions (e.g., Jenner, 2002). Early work suggests that Fe-nitride-catalyzed Fischer–Tropsch gas synthesis rates increase as pressure rises over tens of atmospheres (Anderson et al., 1964), and recent studies suggest that pressure accelerates the thermal decomposition of coal to form light hydrocarbons from 0.5 to 2.5 kbar (Shuai et al., 2006; Tao et al., 2010). Most previous measurements of aqueous methane kinetics have been performed isobarically in flexible-cell hydrothermal apparatus within a relatively restricted pressure range of ~200–500 bars (e.g., Berndt et al., 1996; Horita and Berndt, 1999; McCollom and Seewald, 2001; Foustoukos and Seyfried, 2004; Fu et al., 2008; McCollom et al., 2010; Lazar et al., 2012). Such pressure limitations are partly due to scientific interests in terrestrial seafloor hydrothermal systems, but also to technical limits of the apparatus (Seyfried et al., 1987). Consequently, the effect of pressure on aqueous methanogenesis kinetics has not yet been explicitly investigated, despite the fact that the stability of CH_4-rich fluids is only weakly dependent on pressure (e.g., Fig. 1), indicating that conditions favorable for methane generation extend to lithospheric pressures well in excess of seafloor conditions. Moreover, abundant field evidence suggests that natural abiotic methanogenesis can occur at pressures above 500 bars in a variety of environments: e.g., in the serpentinized

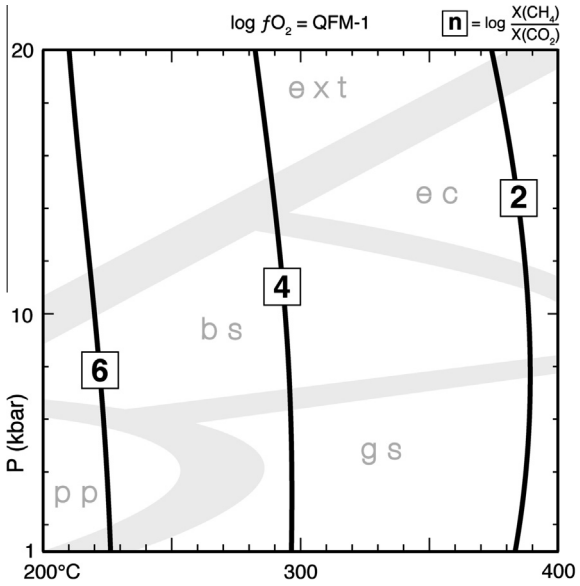

Fig. 1. Isopleths of equilibrium $\log(X_{CH4}/X_{CO2})$ values (solid lines) illustrating the weak pressure-dependence of the stability of methane-rich fluids in the graphite-free C–O–H system from 1 to 20 kbar and 200 to 400 °C, calculated using the CORK equation of state (Holland and Powell, 1991). X = mole fraction; contour interval = two log units; $\log fO_2 = \Delta$QFM-1, where QFM = quartz-fayalite-magnetite; $X_C = 0.0001$. Light gray curves are metamorphic facies boundaries (Spear, 1993); pp = prehnite-pumpellyite(+zeolite), gs = greenschist, bs = blueschist, ext = extraterrestrial.

forearc mantle wedge (Hyndman and Peacock, 2003; Mori et al., 2003; Shi et al., 2005; Sachan et al., 2007; Song et al., 2009), alkalic igneous complexes (Potter et al., 1998, 2004), prograde alpine serpentinites (Peretti et al., 1992), the oceanic mantle lithosphere (Li and Lee, 2006), and Precambrian crystalline basements (Sherwood-Lollar et al., 2002).

Previous experimental and theoretical studies consistently show that methane stability extends to upper mantle conditions and that methane can form experimentally at high P and T and low fO_2 via multiple pathways such as calcite or CO_2 reduction, graphite hydrogenation, and carbon depolymerization (Kenney et al., 2002; Scott et al., 2004; Chen et al., 2008; Kolesnikov et al., 2009; Sharma et al., 2009). Nevertheless, because concentrations were not measured, such experiments yield little quantifiable information on the kinetics of methanogenesis at elevated pressure. Here, we present a series of experiments designed to measure the kinetic pressure effect on aqueous methanogenesis via the model reaction

$$4H_2 + CO_2 = CH_4 + 2H_2O \quad (1)$$

The results suggest that pressure may be an important kinetic variable during methanogenesis in reducing terrestrial and extraterrestrial settings, particularly when the influence of other variables is diminished.

2. MATERIALS AND METHODS

The experiments were performed from 1 to 3.5 kbar at 300 °C for two weeks (336 h) in cold-seal hydrothermal

bombs with an H_2O pressure medium (Tuttle, 1949). Gold was selected as the capsule material due to its effective impermeability to H_2 at the experimental conditions (Chou et al., 1978) and due to its putative unreactivity with C–O–H fluids as interpreted from previous blank experiments (e.g., Berndt et al., 1996; McCollom and Seewald, 2001). Four series of experiments were performed, each using 0.7-inch-long, 2-mm-diameter capsules cut from the same stock of 12-inch-long gold tubing. The inside of each capsule was cleaned with acetone to remove any residual oil used during manufacturing. The capsules used in Series 1, 2, and 3 were cleaned for 6–12 h with a magnetic stirrer in a glass beaker containing hot nitric acid. The capsules used in Series 4 were not cleaned in acid in order to evaluate the effect of acid cleaning on CH_4 yields. Prior to loading the solutions, each batch of capsules was annealed for ~30 min at 900 °C in a box furnace in order to increase capsule pliability and to volatilize any acetone residue or other organic contaminants that survived the hot acid. All capsules within a given experimental series were cleaned and annealed together in the same batch.

The starting fluids were 70-mmolal solutions of ^{13}C-labeled formic acid ($H^{13}COOH$, >99% pure, Cambridge Isotope Labs) in ultrapure H_2O (18 MΩ). At the experimental conditions, $H^{13}COOH$ decomposes rapidly and completely to H_2 and $^{13}CO_2$ (Yu and Savage, 1998), providing the reactants for Reaction (1). Because the natural abundance of ^{13}C is very low, the use of $H^{13}COOH$ permitted the approximation that all $^{13}CH_4$ was generated by $^{13}CO_2$ reduction (McCollom and Seewald, 2001) and that all $^{12}CH_4$ was generated by thermal decomposition of unlabeled organic contaminants. The use of labeled carbon is critical in experimental studies of aqueous alkanogenesis due to the difficulty of eliminating organic contaminants and the consequent potential for ambiguity in identifying the source of alkane products. Possible sources of unlabeled contaminants include residual acetone and machining oil that survived volatilization at 900 °C, and trace organics in the starting fluid.

The capsules were sealed with a DC arc welder under Ar gas. Duplicate or triplicate experiments at identical conditions were contained within the same cold-seal bomb (e.g., 05A and 05B). The quench time from 300 °C to below 100 °C was 10–15 min. After quenching, each capsule was wiped clean with ethanol and H_2O, weighed to confirm mass conservation, and then placed in a 6-mL gas vial sealed with an airtight rubber septum. Prior to puncturing each capsule with a needle, a 50–100-mTorr vacuum was generated in the vial to promote volatile release from the capsule.

After puncturing, the liberated volatiles were extracted in multiple aliquots using a 2.5-mL locking gas syringe and immediately injected into an Agilent 6890 coupled gas chromatograph mass spectrometer (GCMS) equipped with a CarbonPlot column. The total amounts of methane and ethane in each experiment were computed by summing the amounts in each vial extraction. For each experiment, extractions were repeated until a given aliquot contained less than 1% of the cumulative total of methane, a criterion typically satisfied after 10–15 extractions. GCMS analyses were performed at a runtime of 3.5 min and an oven temperature of 75 °C. Calibration curves were constructed from analyses of unlabeled calibration gas with known CH_4 and C_2H_6 partial pressures. Linear chromatographic responses were confirmed by a series of calibration analyses that were colinear with the origin. Five analyses of unlabeled calibration gas were averaged to construct normalized standard mass spectra for CH_4 and C_2H_6 (Fig. 2). The methane and ethane detection limits were, respectively, 0.6 and 0.3 μmolal.

The extracted ion chromatograms (EICs) for methane revealed interference at mass 16 by a strong signal from $^{16}O^+$ on the shoulder of the air peak. To avoid correcting for $^{16}O^+$, methane concentrations were quantified using interference-free masses 15 and 17. Unlabeled methane was calibrated at mass 15 (Fig. 3A), and the experimental fluids were analyzed at masses 15 and 17 (Fig. 3B). Ethane was calibrated at mass 30 and measured in the fluids at interference-free masses 26, 29, and 30. Mass 28 was excluded due to interference from $^{14}N_2^+$ in air.

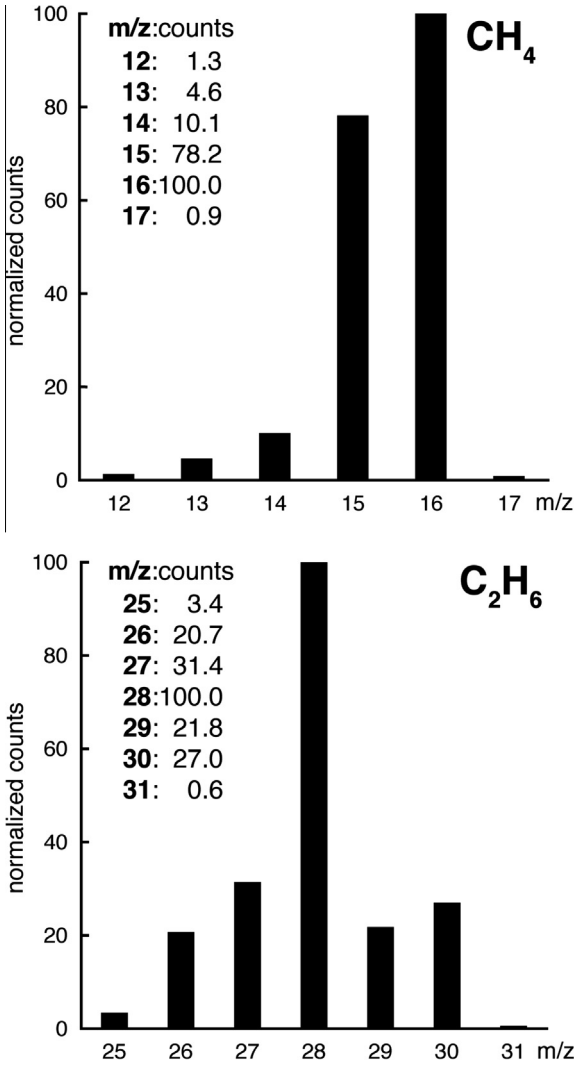

Fig. 2. Normalized mass spectra of unlabeled CH_4 and C_2H_6, constructed by averaging five GCMS analyses of calibration gas.

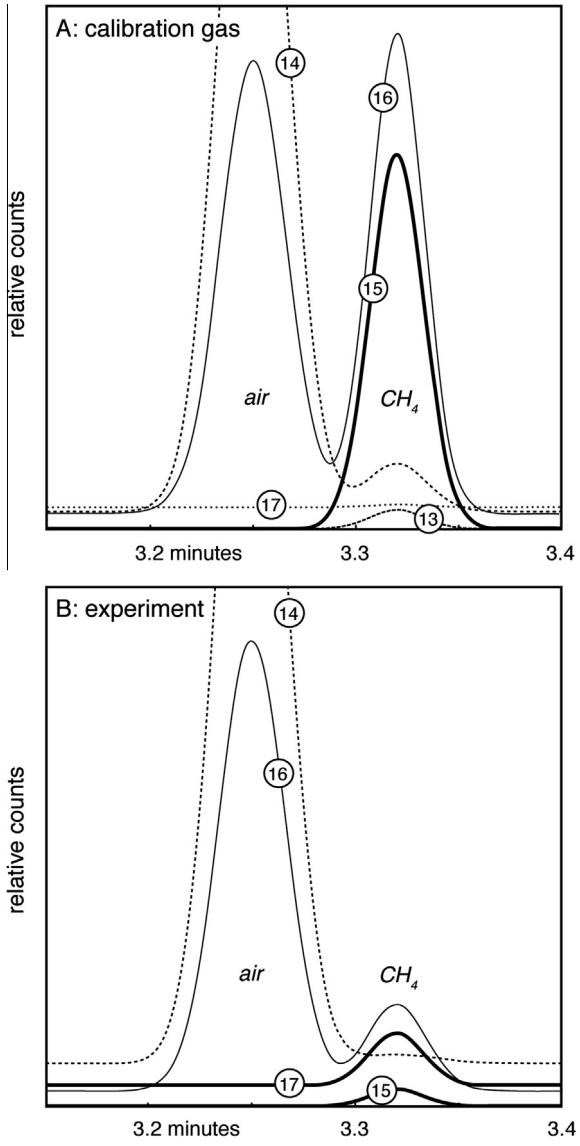

Fig. 3. Representative extracted ion chromatograms (EICs) over the mass range 13–17 for unlabeled CH_4 in the calibration gas (A) and an experiment containing labeled methane (B). Ion masses are shown in open circles. Masses with symmetrical peaks used for calibration and experimental analyses are shown with solid lines: 15 in (A); 15 and 17 in (B).

The mass spectra of experimentally generated methane represented mixtures of labeled and unlabeled species. For example, the signal at mass 15 represented a mixture of $^{12}CH_3^+$ and $^{13}CH_2^+$ ions and the CH_4 signal at mass 17 represented a mixture of $^{12}CH_5^+$ and $^{13}CH_4^+$ ions. Values for $[^{13}CH_4]$, $[^{12}CH_4]$, and total $[CH_4]$ could be computed by simultaneously solving four expressions for the bulk concentrations measured in the EICs at masses 15 and 17 and the measured ion count ratios $^{12}CH_3^+$:$^{12}CH_5^+$ and $^{13}CH_2^+$:$^{13}CH_4^+$. The unlabeled count ratio, $^{12}CH_3^+$:$^{12}CH_5^+$, was measured directly in the unlabeled calibration gas. The labeled count ratio, $^{13}CH_2^+$:$^{13}CH_4^+$, was assumed to be equal to the unlabeled ratio, $^{12}CH_2^+$:$^{12}CH_4^+$, also measured in the calibration gas. Both unlabeled ratios were found to be constant within uncertainty over a range of CH_4 partial pressures that overlapped the experimental measurements. Experimental ethane had three potential isotopologues: $^{12}C_2H_6$, $^{12}C^{13}CH_6$, and $^{13}C_2H_6$. Whereas solving for $[^{13}CH_4]$ and $[^{12}CH_4]$ required two ion chromatogram measurements and two ion ratio measurements, solving for $[^{12}C_2H_6]$, $[^{12}C^{13}CH_6]$, and $[^{13}C_2H_6]$ required three ion chromatograms (masses 26, 29, and 30) and six corresponding ion ratios. As with methane, ratios between labeled ions were assumed to be equal to the corresponding unlabeled ion ratios in the calibration gas: e.g., $^{12}C_2H_4^+$:$^{12}C_2H_5^+$ was assumed to be equal to $^{13}C^{12}CH_4^+$:$^{13}C^{12}CH_5^+$.

X-ray fluorescence (XRF) was used to analyze the composition of the inner wall of the gold capsules. Four samples of the gold stock were analyzed; two were cleaned in double distilled, ultrapure concentrated HCl for 6 days at 120 °C in sealed Teflon beakers and two were not cleaned in acid. Data were collected on randomly selected points for 2000 live seconds at 40 kV and 1 mA. The X-ray detector was an EDAX 30 mm^2 Si(Li) detector with a 25-μm-thick Be window. Spectra were collected at the 25.6 μs time constant, which has a standard energy calibration of 10 eV/ch and a resolution of approximately 140 eV. A 50-μm-thick Rh foil was used to reduce X-ray scattering in the 3–10-keV region. Standard spectra were collected on pure Cu and pure Au from NIST SRM 482. The Fe detection limit was 50 ppm.

Except as noted in Fig. 1, all thermodynamic calculations were performed using SUPCRT92 (Johnson et al., 1992) and the slop98 database (geopig.asu.edu). Unit activity was assumed for all solid phases relative to a standard state of the pure solid at P and T. The standard state for gases was the pure gas at T and 1 bar. Fugacity coefficients were computed using the CORK equation of state (Holland and Powell, 1991). Mixing of real gases was assumed to be ideal at all P and T (Lewis and Randall, 1923). The standard state for aqueous species was a hypothetical one-molal solution referenced to infinite dilution. Because aqueous reactions were modeled in pure H_2O at low P ($\leqslant$3.5 kbar) where ionic strength is low, activity coefficients for aqueous species were assumed to be unity.

3. RESULTS

The experimental results are presented in Table 1. No more than three major peaks were observed in the total ion chromatogram of any given experiment and each peak could be attributed to CH_4, CO_2, or air.

3.1. Methane

Labeled methane was detected in all experiments. In a majority of experiments, greater than 50% of the total methane was $^{13}CH_4$. Three types of variation in $[^{13}CH_4]$ were observed (Fig. 4A). First, application of pressure caused a reproducible increase in $[^{13}CH_4]$ in all series. This pressure effect could be quantified by the log-linear regression slope, m, where

$$m = \frac{\Delta \log[^{13}CH_4]}{\Delta P} \quad (2)$$

Table 1
Experimental conditions and results.

Run	P	$H^{13}COOH$ solution	Initial $^{13}CO_2$	$^{13}CH_4$ generated	$[^{13}CH_4]$	$^{12}CH_4$ generated	$[^{12}CH_4]$	Conversion of $^{13}CO_2$[a]	$\%^{13}CH_4$[b]	Resolvable C_2H_6 masses[c]	Total $[C_2H_6]$	$[^{13}C_2H_6]$[d]		$[^{13}C^{12}CH_6]$[d]		$[^{12}C_2H_6]$[d]	
	kbar[e]	mg[f]	nmoles	nmoles	mmolal	nmoles	mmolal	%	%	*m/z*	μmolal[g]	μmolal[g]	%[g]	μmolal	%	μmolal[g]	%
Series 1																	
05A	1.5	20.4	1428 ± 38	0.40 ± 0.05	0.02 ± 0.00	0.37 ± 0.02	0.02 ± 0.00	0.03 ± 0.00	52 ± 08	b.d.[*]	–	–	–	–	–	–	–
05B	1.5	20.8	1456 ± 38	0.60 ± 0.04	0.03 ± 0.00	3.25 ± 0.06	0.16 ± 0.00	0.04 ± 0.00	16 ± 01	b.d.	–	–	–	–	–	–	–
06A	2.5	20.7	1449 ± 38	1.58 ± 0.11	0.08 ± 0.01	0.43 ± 0.01	0.02 ± 0.00	0.11 ± 0.01	78 ± 07	b.d.	–	–	–	–	–	–	–
06B	2.5	20.9	1463 ± 38	5.36 ± 0.36	0.26 ± 0.02	1.40 ± 0.05	0.07 ± 0.00	0.37 ± 0.03	79 ± 07	b.d.	–	–	–	–	–	–	–
07A	3.5	21.1	1477 ± 39	18.89 ± 1.02	0.90 ± 0.05	5.77 ± 0.15	0.27 ± 0.01	1.28 ± 0.08	77 ± 05	26,30	–[**]	–	–	–	–	–	–
07B	3.5	21.0	1470 ± 39	9.68 ± 0.45	0.46 ± 0.02	6.89 ± 0.12	0.33 ± 0.01	0.66 ± 0.04	58 ± 03	b.d.	–	–	–	–	–	–	–
Series 2																	
08A	1	21.0	1470 ± 39	0.28 ± 0.02	0.01 ± 0.00	4.68 ± 0.09	0.22 ± 0.00	0.02 ± 0.00	6 ± 00	26,30	–[**]	–	–	–	–	–	–
08B	1	21.1	1477 ± 39	0.72 ± 0.04	0.03 ± 0.00	4.06 ± 0.08	0.19 ± 0.00	0.05 ± 0.00	15 ± 01	26,30	–[**]	–	–	–	–	–	–
09A	2	20.8	1456 ± 38	3.57 ± 0.18	0.17 ± 0.01	5.64 ± 0.09	0.27 ± 0.00	0.25 ± 0.01	39 ± 03	26,29,30	19.1	0.8	4%	6.5	35%	11.9	61%
09B	2	20.9	1463 ± 38	6.42 ± 0.25	0.31 ± 0.01	11.92 ± 0.25	0.57 ± 0.01	0.44 ± 0.02	35 ± 02	26,30	–[**]	–	–	–	–	–	–
10A	3	20.8	1456 ± 38	16.02 ± 0.65	0.77 ± 0.03	10.03 ± 0.15	0.48 ± 0.01	1.10 ± 0.05	62 ± 03	25,26,27,29,30,31	28.5	0.8	3%	10.9	38%	16.9	59%
Series 3																	
14A	1	21.2	1484 ± 39	2.38 ± 0.31	0.11 ± 0.01	0.36 ± 0.03	0.02 ± 0.00	0.16 + 0.02	87 ± 15	b.d.	–	–	–	–	–	–	–
14B	1	20.4	1428 ± 38	1.02 ± 0.12	0.05 ± 0.01	0.45 ± 0.02	0.02 ± 0.00	0.07 ± 0.01	69 ± 10	26,30	–[**]	–	–	–	–	–	–
14C	1	19.7	1379 ± 36	2.08 ± 0.26	0.11 ± 0.01	0.40 ± 0.03	0.02 ± 0.00	0.15 ± 0.02	84 ± 14	b.d.	–	–	–	–	–	–	–
15B	2.25	21.2	1484 ± 39	17.54 ± 1.79	0.83 ± 0.08	1.23 ± 0.18	0.06 ± 0.01	1.18 ± 0.13	93 ± 13	25,26,27,29,30	31.0	1.1	5%	2.3	5%	27.7	90%
15C	2.25	21.3	1491 ± 39	23.72 ± 2.61	1.11 ± 0.12	1.55 ± 0.25	0.07 ± 0.01	1.59 ± 0.18	94 ± 14	26,30	–[**]	–	–	–	–	–	–
16A	3.5	21.3	1491 ± 39	30.81 ± 3.32	1.45 ± 0.16	2.09 ± 0.33	0.10 ± 0.02	2.07 ± 0.23	94 ± 14	26,29,30,31	18.1	15.6	88%	0	0%	2.5	12%
16B	3.5	20.8	1456 ± 38	44.62 ± 3.91	2.15 ± 0.19	2.37 ± 0.37	0.11 ± 0.02	3.06 ± 0.29	95 ± 12	26,30	–[**]	–	–	–	–	–	–
16C	3.5	20.6	1442 ± 38	96.78 ± 7.87	4.70 ± 0.38	4.97 ± 0.75	0.24 ± 0.04	6.71 ± 0.58	95 ± 11	26,29,30	16.4	10.7	65%	0	0%	5.7	35%
Series 4																	
17A	2	20.0	1400 ± 37	13.33 ± 0.97	0.67 ± 0.05	1.60 ± 0.10	0.08 ± 0.01	0.95 ± 0.07	89 + 09	b.d.	–	–	–	–	–	–	–
18A	3	20.5	1435 ± 38	46.63 ± 2.98	2.27 ± 0.15	5.62 ± 0.30	0.27 ± 0.01	3.25 ± 0.23	89 + 08	26,30	–[**]	–	–	–	–	–	–

Temperature = 300 °C. Time = 336 h (two weeks). Initial $[H^{13}COOH] = 69.6 \pm 1.8$ millimolal.

[a] Proportion of $^{13}CH_4$ relative to initial $^{13}CO_2$.

[b] Proportion of $^{13}CH_4$ relative to total CH_4.

[c] Ethane masses that were resolvable from background in extracted ion chromatograms within the *m/z* range 25–31.

[d] Concentrations of ethane isotopologues were computed by multiplying total $[C_2H_6]$ by proportion factors derived from mass spectra of calibrated gas (see Section 2).

[e] Uncertainty = ± 0.05 kbar.

[f] Uncertainty = ± 0.1 mg.

[g] Uncertainty = ± 10–20%.

[*] b.d.: below detection.

[**] Total $[C_2H_6]$ and isotopologue concentrations could not be calculated because fewer than three masses were resolvable in the extracted ion chromatograms (see Section 2).

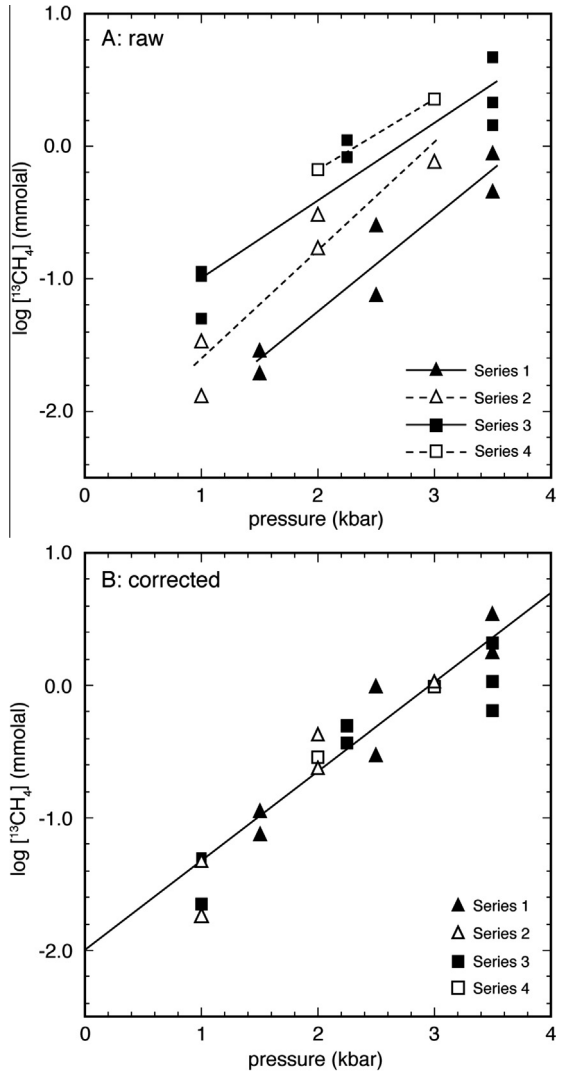

Fig. 4. Log [$^{13}CH_4$] versus pressure, 300 °C, two weeks. (A) Raw data. (B) Corrected to mean regression. Solid and dashed lines in (A) are unweighted regressions. Solid line in (B) is the mean regression. Error bars are not visible at this scale.

with units of log mmolal per kbar. The slopes of all series were within one standard error (s.e.) of the average slope (Table 2), indicating good reproducibility. To refine the uncertainty in the average slope, each series was corrected to fit the mean regression (Fig. 4B). Regression of the corrected composite dataset yielded a slope of 0.66 ± 0.05 (±1 s.e.) log mmolal per kbar.

The second type of variation in [$^{13}CH_4$] occurred between pairs and triplets of experiments performed simultaneously at identical conditions within the same pressure vessel. Within the pairs and triplets, [$^{13}CH_4$] varied by as much as 0.5 log units, generating scatter about the mean regression. This scatter did not substantially compromise a good fit of the regressions: R^2 values for Series 1 through 3 were approximately 0.9.

The third type of variation was observed as differences between the *y*-intercepts of the regressions of each series.

Table 2
Unweighted linear regression analyses of log [$^{13}CH_4$] versus pressure.

Set	*N*	Slope	±1se	*y*-Int	±1se	R^2
[$^{13}CH_4$]						
1	6	0.72	0.11	−2.68	0.29	0.91
2	5	0.82	0.15	−2.42	0.29	0.91
3	8	0.59	0.08	−1.59	0.20	0.90
4	2	0.53	0.11[†]	−1.24	n/a	n/a
All[‡]	21	0.66	0.05	−2.02	0.13	0.89

N = number of data points.
[†] Uncertainty averaged from the uncertainty of the other three series.
[‡] All = composite regression of all [$^{13}CH_4$] data from Sets 1–4 corrected to fit the mean slope and intercept. Units of regressions are log mmolal versus kbar. Errors are propagated absolute uncertainties.

Despite the similar pressure ranges of the series, the *y*-intercepts varied by as much as 1.8 log units, e.g., between Series 2 and 4. Series 4, which was performed using capsules that were not acid-cleaned, had the highest *y*-intercept of all.

As with $^{13}CH_4$, application of pressure caused an increase in [$^{12}CH_4$] (Table 1, Fig. 5). The average slope of the $^{12}CH_4$ data was 0.36 log mmolal per kbar, roughly half the average slope of the $^{13}CH_4$ data. In Series 2–4, [$^{12}CH_4$] increased systematically with pressure. Despite substantial scatter, the Series 1 slope (0.34 log mmolal per kbar) was similar to the average slope. The [$^{12}CH_4$] intercepts did not correlate to the [$^{13}CH_4$] intercepts; e.g., Series 1 had the highest [$^{12}CH_4$] intercept but the second lowest [$^{13}CH_4$] intercept. The proportion of $^{13}CH_4$ relative to $^{12}CH_4$ increased with *P* in Series 2, but was pressure-independent in the other series.

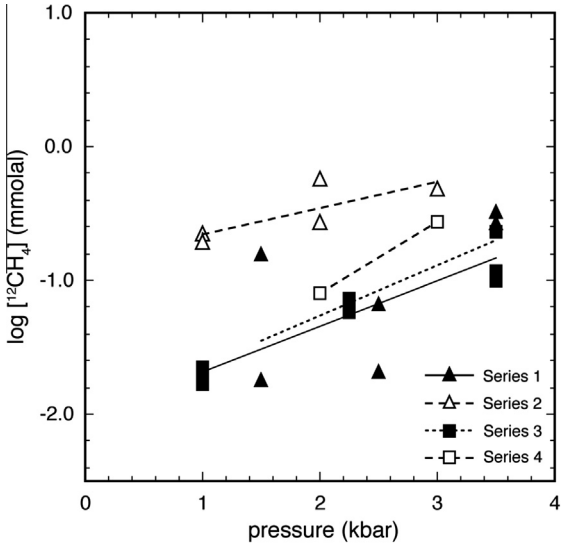

Fig. 5. Log [$^{12}CH_4$] versus pressure, 300 °C, two weeks. Solid and dashed lines are unweighted semi-log regressions. Error bars are not visible at this scale.

3.2. Ethane

Ethane was detected in the EICs of a majority of the experiments (Table 1), but at much lower concentrations than methane. The concentration and proportion of ethane isotopologues could be quantified in only five experiments, each of which satisfied the analytical requirement of three resolvable ions (see Materials and Methods). In these experiments, the isotopic composition of ethane was highly variable, ranging from mostly unlabeled (15B) to mostly ^{13}C-labeled (16A) (Table 1, Fig. 6). In another eight experiments, ethane EICs were only resolvable at masses 26 and 30, preventing calculation of the proportions of component isotopologues. In 8 out of 21 experiments, ethane was below detection at all masses. With the caveat that the ethane data are limited, the results of Series 2 and 3 suggest a pressure effect on ^{13}C-labeled ethane yields (Fig. 7), wherein the total ^{13}C-bearing ethane concentration, $[^{13}C_2H_6]+[^{13}C^{12}CH_6]$, increased by an average slope of

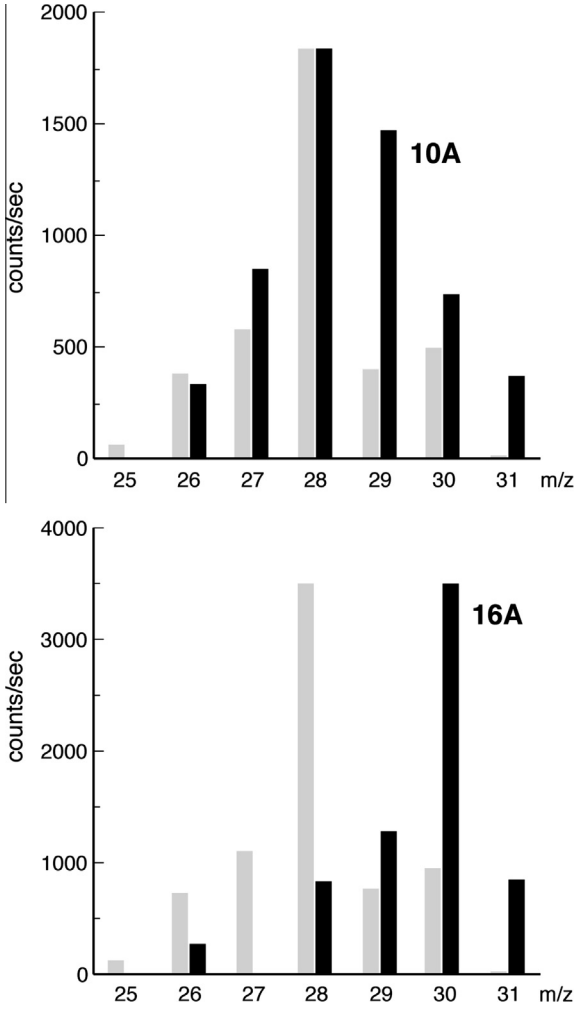

Fig. 6. Selected mass spectra of ^{13}C-bearing ethane generated in experiment 10A (top) and 16A (bottom). Experimental mass spectra are shown in black; averaged spectra of the unlabeled calibration gas are shown in gray.

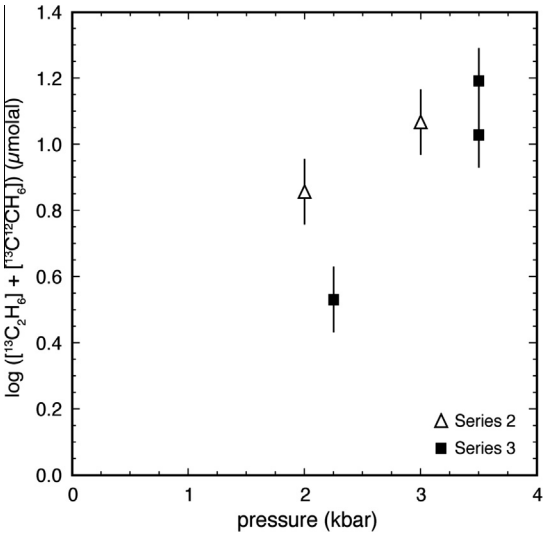

Fig. 7. Log concentration of ^{13}C-labeled ethane versus pressure, 300 °C, two weeks. The concentration of ^{13}C-labeled ethane was computed by adding the concentrations of partially labeled ($^{13}C^{12}CH_6$) and fully labeled ($^{13}C_2H_6$) ethane.

0.3–0.4 log μmolal per kbar. Consistent with this observation, total ^{13}C-labeled ethane in Series 2 and 3 was below detection only at the lowest pressures.

3.3. XRF analyses

XRF analyses revealed the presence of trace, variable Fe on the inner capsule walls. Of the two capsule samples that were not acid-cleaned, one contained an estimated 50–200 ppm Fe and the other contained no detectable Fe. Neither of the two acid-cleaned gold capsules contained detectable Fe. No other elements besides Au and Fe were detected in any capsule sample. These results suggest that Fe was heterogeneously distributed in the uncleaned capsules and that the abundance of Fe decreased after cleaning in acid.

4. DISCUSSION

4.1. Pressure-independent effects: heterogeneous catalysis by Fe

Native Fe has been previously shown to strongly catalyze methanogenesis (Horita and Berndt, 1999; McCollom et al., 2010). If the trace amount of Fe in the capsule wall affected [$^{13}CH_4$], then the *y*-intercept of a given series would inversely correlate to the extent of acid leaching of Fe from the corresponding batch of gold capsules. This hypothesis is supported by the results of Series 4, wherein the time of cleaning was zero and the *y*-intercept was the highest. Iron catalysis can also explain [$^{13}CH_4$] variations in duplicate experiments, e.g., 06A and 06B, as a consequence of spatial variability of Fe in the Au tube stock, possibly due to random streaks produced by the abrasion of steel machine tools during the manufacturing process.

4.2. Assessing mechanisms for the pressure effect on [$^{13}CH_4$]

Below, several hypotheses are tested in order to constrain the mechanism(s) responsible for the observed pressure effect on methane yields. It is not possible in the present study to narrow the hypotheses to a single mechanism; however, thermodynamic calculations, empirical observations, and inferences from previous work permit the elimination of several possibilities in favor of one or more of the following three processes: reduction of metastable methanol, Fe-carbonyl formation in the fluid, and/or heterogeneous catalysis by Fe.

4.2.1. Homogeneous equilibrium

To test for homogeneous equilibrium in the C–O–H system, experimental [CH_4] values were compared to calculated equilibrium values. The experimental [CH_4] values were computed as the sum of [$^{12}CH_4$] and [$^{13}CH_4$]. The equilibrium [CH_4] values were computed for a single phase, dilute H_2O fluid by reacting the initial fluid composition ([CO_2] = [H_2] = 70 mmolal) stoichiometrically via Reaction (1) until the reaction quotient equaled the equilibrium constant. All experimental [CH_4] values were far below the calculated equilibrium values (Fig. 8), indicating that homogeneous equilibrium cannot explain the observed methane yields.

4.2.2. Graphite saturation

Methane stability in the C–O–H system is enhanced by pressure when graphite is saturated (French, 1966); therefore, the pressure-induced increase in [$^{13}CH_4$] may have been a consequence of graphite-fluid equilibria. Although graphite was not observed in any experiment, the possibility of its cryptic precipitation was assessed by computing the bulk mole fraction of carbon (X_C) required for graphite-fluid equilibrium as fixed by the total [CH_4] values measured in each experiment. The calculations show that the computed X_C values at graphite saturation were about 100 times higher than the actual X_C values in the experiments (Fig. 9), indicating that graphite-fluid equilibria cannot explain the experimental CH_4 concentrations.

4.2.3. Gas phase reaction

It has been proposed that reaction in a gas phase can accelerate hydrothermal methanogenesis (McCollom and Seewald, 2001). However, measured [CH_4] values in all experiments were far below methane gas saturation (>1 wt%) in the system CH_4-H_2O at 300 °C (Bonham, 1978). Moreover, the experiments were below H_2 gas saturation, as shown by plotting experimental [H_2] values on an isothermal P–X_{H2} phase diagram in the system H_2–H_2O at 300 °C and 0.3–2.5 kbar (Fig. 10, adapted from Seward and Franck, 1981). The experimental [H_2] values were estimated to be 100 mmolal ($X_{H2} = 0.002$), as derived from the assumption of 100% decomposition of the initial formic acid (70 mmolal) plus 30 mmolal from the generous estimate that additional hydrogen formed by oxidation of 200 ppm Fe in a 100-micron-thick layer along the inner capsule wall. Nevertheless, even this likely overestimated [H_2] value is far below gas saturation from 1 to 2.5 kbar, and to 3.5 kbar with a modest extrapolation (Fig. 10).

4.2.4. Mediation by background organics

The observed pressure effect on [$^{12}CH_4$] (Fig. 5) suggests that [$^{13}CH_4$] may have been modulated by interaction of ^{13}C with unlabeled organic contaminants. If true, then there would be a systematic dependence of [$^{13}CH_4$] on [$^{12}CH_4$] throughout the entire dataset. However, a plot of [$^{13}CH_4$] versus [$^{12}CH_4$] reveals highly variable slopes between the

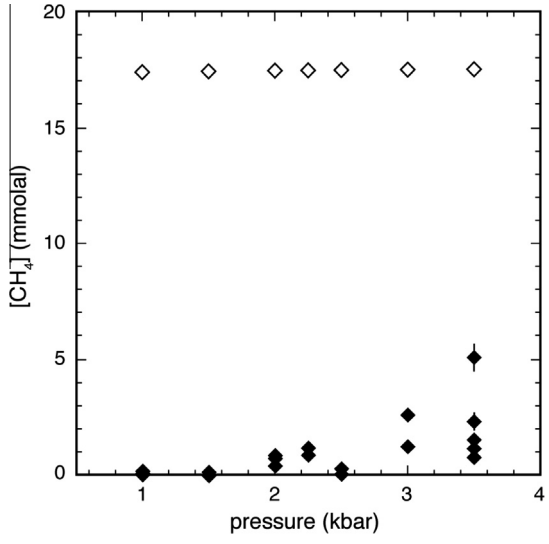

Fig. 8. Comparison of experimental [CH_4] (filled diamonds) to computed [CH_4] in equilibrium with H_2 and CO_2 (open diamonds). Experimental [CH_4] includes labeled and unlabeled species. See Section 4.2.1.

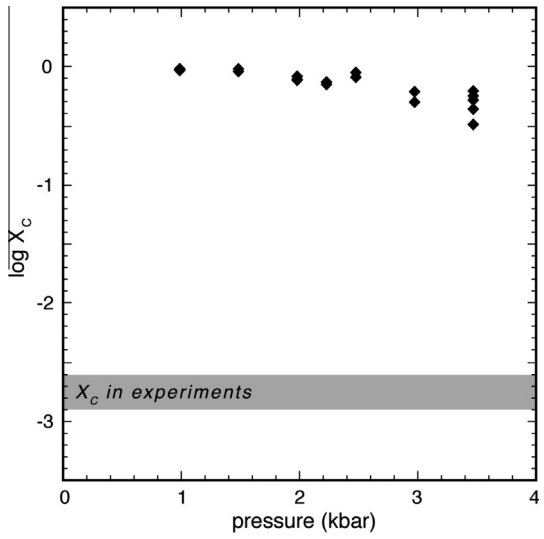

Fig. 9. Mole fraction of carbon (X_C) required for graphite saturation in each experiment (filled diamonds), where $X_C = -X_{CO2} + X_{CH4}$ (CO is assumed to be a trace species). The grey horizontal region represents the actual range of experimental bulk carbon values, computed as [$^{13}CH_4$] + [$^{12}CH_4$] with a generous estimate for the upper limit. Error bars are not visible at this scale. See Section 4.2.2.

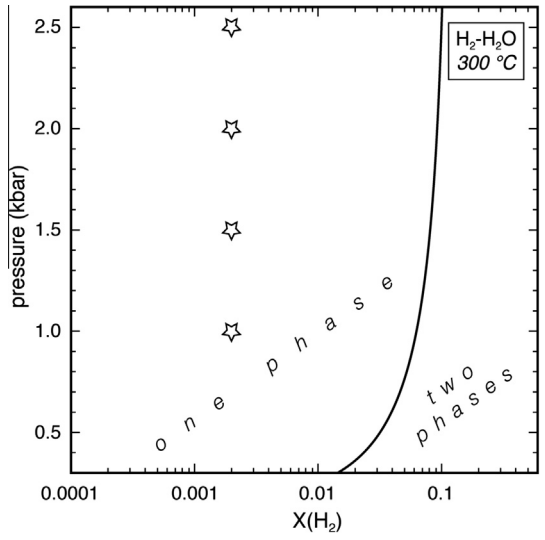

Fig. 10. Selected experimental conditions (open stars) superimposed on phase equilibria in the system H_2–H_2O, 300 °C. Error bars are not visible at this scale. See Section 4.2.3.

series (Fig. 11), from a maximum of ~60 (Series 3) to a minimum of ~1 (Series 2), indicating no systematic relationship between labeled and unlabeled methane concentrations. A likely explanation for the observed pressure enhancement of [$^{12}CH_4$] is a pressure effect on thermal cracking of background organics, a phenomenon that has been observed in previous experiments on coal pyrolysis (e.g., Shuai et al., 2006; Tao et al., 2010).

4.2.5. Pressure-dependent C–O–H speciation

Aqueous methanogenesis has been proposed to occur via the following sequence of reaction intermediates: CO_2 /CO → HCOOH → CH_2O → CH_3OH → CH_4

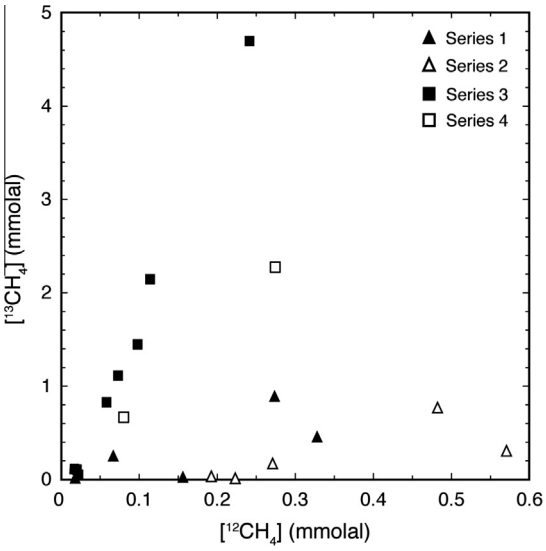

Fig. 11. Labeled methane concentrations, [$^{13}CH_4$], versus unlabeled methane concentrations, [$^{12}CH_4$]. Error bars are not visible at this scale. See Section 4.2.4.

(Seewald et al., 2006). In an equilibrated H_2-rich fluid, the concentrations of such intermediates are low because most carbon is speciated as CH_4. However, because methanogenesis is much slower than the generation of intermediate species, the intermediates may accumulate in solution at concentrations governed by metastable, CH_4-suppressed equilibria (Shock, 1990, 1992; McCollom and Seewald, 2001, 2003; Seewald et al., 2006). In a previous hydrothermal flexible-cell experiment at 200 °C and 350 bar (Seewald et al., 2006), maximum [CH_4] was coincident with maximum [CH_3OH], suggesting that methane concentrations were rate-limited by the reduction of metastable methanol via the reaction:

$$CH_3OH + H_2 = CH_4 + H_2O \quad (3)$$

It is possible, therefore, that the pressure effect on [$^{13}CH_4$] was due to pressure-dependent variations in the concentrations of a rate-limiting, metastable intermediate species such as methanol.

Metastable speciation calculations for a CH_4-suppressed C–O–H fluid at 300 °C from 1 to 3.5 kbar reveal a significant pressure effect (Fig. 12). For example, at pH = 5, CO_2 is the most abundant C-bearing species at 1 kbar, but CH_3OH predominates at 3.5 kbar. To quantify the relative pressure effect, ratios of selected species were computed from 1 to 3.5 kbar, and normalized to the same ratios at 1 kbar (Fig. 13). Fig. 13A shows that the relative concentrations of pH-independent metastable species increase with pressure, and methanol shows the largest increase. The pressure effect on the relative concentrations of pH-dependent metastable species is highly variable (Fig 13B), as illustrated by an analysis of the ratio, [ΣHCOOH]:[ΣCO_2], where

$$\left[\sum \mathrm{HCOOH}\right] = [\mathrm{HCOOH}] + [\mathrm{HCOO^-}] \quad (4)$$

and,

$$\left[\sum \mathrm{CO_2}\right] = [\mathrm{CO_2}] + \left[\mathrm{HCO_3^-}\right] + \left[\mathrm{CO_3^{2-}}\right] \quad (5)$$

For example, as P increases, [ΣHCOOH]:[ΣCO_2] increases at pH = 6, but decreases at pH = 11. Although the influence of formate species on $^{13}CH_4$ yields cannot be ruled out, previous work at lower pressure has shown no relationship between [ΣHCOOH] and [CH_4] (Seewald et al., 2006).

4.2.6. Fluid-hosted Fe-carbonyls

Pressure may have increased $^{13}CH_4$ yields by promoting reaction of the fluid with Fe in the capsules to form fluid-hosted (i.e., not surface-bound) iron carbonyl complexes (e.g., $Fe(CO)_5$), following a reaction such as

$$Fe^{\circ} + 5CO = Fe(CO)_5 \quad (6)$$

Due to limited thermodynamic data for Fe-carbonyls and limited compositional constraints, it is not possible to model carbonyl formation in the present experiments. Nevertheless, previous hydrothermal studies at broadly similar conditions have shown that the stability of fluid-hosted Fe-carbonyl complexes increases with pressure (Cody et al., 2000, 2004) and that methane yields are enhanced when immiscible Fe-carbonyls are present (Sharma et al., 2009).

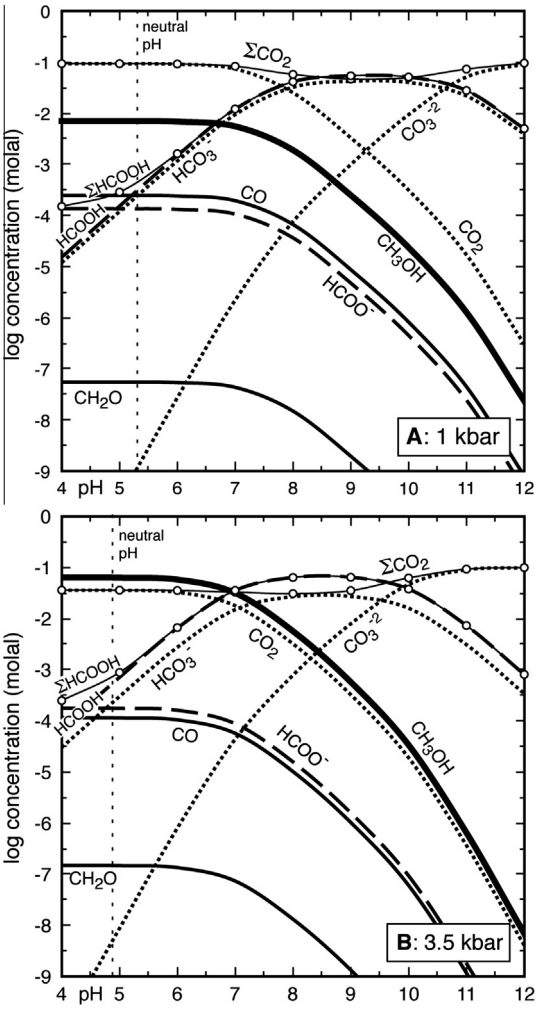

Fig. 12. Metastable, methane-suppressed speciation calculations for a homogeneous C–O–H fluid, 300 °C, 1 kbar (A) and 3.5 kbar (B). Total carbon = 100 mmolal; $[H_2] = 70$ mmolal. $[\Sigma HCOOH] = [HCOOH] + [HCOO^-]$ and $[\Sigma CO_2] = [CO_2] + [HCO_3^-] + [CO_3^{-2}]$. See Section 4.2.5.

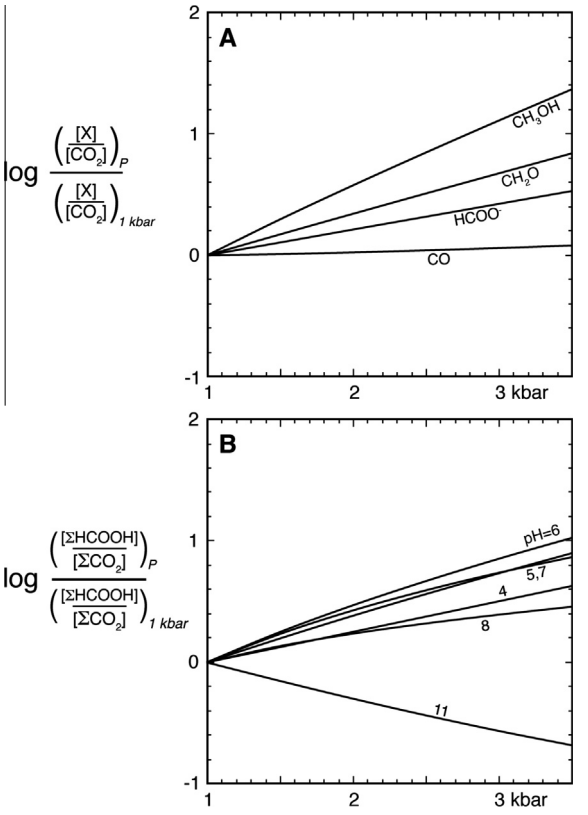

Fig. 13. Relative change in the concentration ratios of selected metastable aqueous species versus pressure at 300 °C. (A) pH-independent variations in concentration ratios of [X]:$[CO_2]$, where X = CH_3OH, CH_2O, $HCOO^-$, or CO. (B) pH-dependent variations in concentration ratios of total formate to total CO_2, where $[\Sigma HCOOH] = [HCOOH] + [HCOO^-]$ and $[\Sigma CO_2] = [CO_2] + [HCO_3^-] + [CO_3^{-2}]$.

4.2.7. Heterogeneous catalysis by Fe

Because C_2H_6 forms cogenetically with CH_4 during Fischer–Tropsch catalysis (Dry, 1981; Anderson, 1984; McCollom and Seewald, 2007), the *P*-dependent increase in ^{13}C-labeled ethane concentration (Fig. 7) provides indirect evidence for a pressure effect on the Fe-catalysis of methane. Although the possibility remains that ^{13}C-labeled ethane formed by homogeneous $^{13}CH_4$ polymerization (McCollom, 2013), previous aqueous hydrothermal syntheses of ^{13}C-labeled ethane have only been observed in the presence of Fischer-Tropsch-type (FTT) transition metal catalysts such as Fe° metal (McCollom and Seewald, 2006), Fe-chromite (Foustoukos and Seyfried, 2004), pentlandite (Fu et al., 2008), and cobalt-bearing magnetite (Ji et al., 2008). Because such studies link ethane generation to Fe-catalysis, the *P*-dependent increase in ^{13}C-labeled ethane concentrations in the present experiments suggests that pressure may have accelerated Fe-catalyzed ethanogenesis and methanogenesis. A kinetic pressure effect on catalysis by Fe could result from a favorable decrease in the activation volume of a surface-bound transition state (Jenner, 2002), e.g., carbonyls or methylene groups (McCollom and Seewald, 2007), or from an increase in the effective solute concentration at the fluid-mineral interface attending compression of the solution.

4.3. Implications for natural systems

It should be emphasized that natural methane yields depend on many other kinetic factors such as temperature, fluid residence time, the presence of catalysts, gas phase reaction, or bulk fluid composition. Nevertheless, a kinetic pressure effect may be important in certain geological environments when the influence of other kinetic factors is diminished. For example, pressure may be important in enhancing methanogenesis in deep extraterrestrial oceans, where it may compensate for otherwise slow kinetics at cold temperatures. Whether methane-stabilizing water–rock interaction occurs on icy planetary bodies is an open question, but numerical modeling of tidal heating and olivine fracturing in Europa suggest that hydrothermal circulation may be active at the seafloor, where pressure may reach 2–3 kbar (Vance et al., 2007).

A kinetic pressure effect may also be important when heterogeneous catalysis is not a factor. Catalysts may become passivated (McCollom and Seewald, 2006, 2007), or may not be present at all. For example, the proposed catalyst, awaruite (Ni_3Fe) (Horita and Berndt, 1999), has a stability range limited to the redox conditions of incipient, partial serpentinization: e.g., the fluid-saturated assemblage, serpentine–olivine–brucite–magnetite, in which fO_2 is buffered 4 to 7 log units below QFM (Frost, 1985; Klein and Bach, 2009). However, the stability range of methane-rich fluids extends to fO_2 values as "high" as QFM, which is considerably more oxidizing than the awaruite stability limit. This broader fO_2 range is accessible to serpentinite assemblages more oxidizing than serpentine–olivine–brucite–magnetite (Frost, 1985) and to other metamorphic processes in the lithosphere such as hydrothermal alteration of basalt (Lyons et al., 2005). In such environments, pressure may compensate for the absence of awaruite or other catalysts by promoting methanol-mediated methanogenesis. The absence of awaruite has been invoked to rule out an abiotic origin for CH_4-rich fluid inclusions in a blueschist-grade jadeitite (Shi et al., 2005), but the above arguments suggest that catalysts in such high pressure environments are unnecessary for substantial methane yields.

The potential for methanol (MOH) generation in geological settings may be evaluated by computing log K_{MOH} values versus P and T for the following reaction:

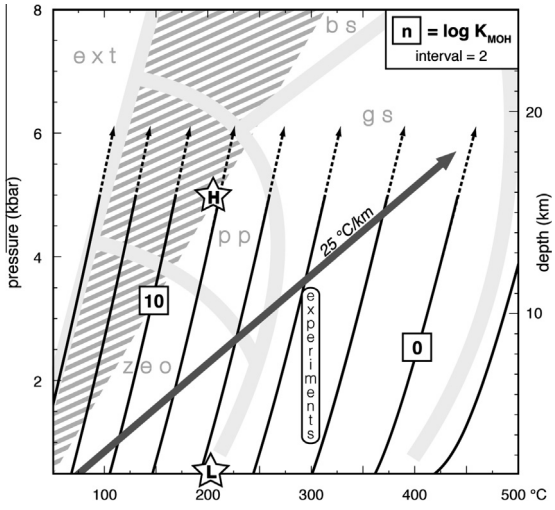

Fig. 14. Log K_{MOH} (Reaction (7)) isopleths at P and T (solid black contours), depicting the thermodynamic drive for metastable methanol formation over a range of geological conditions. Dashed arrows are extrapolated beyond the limit of the slop98.dat database. The medium gray arrow represents an average geothermal gradient, 25 °C/km. Open stars represent conditions consistent with forearc mantle serpentinization (H) and seafloor serpentinization (L). The elongate open symbol denoted by "experiments" depicts the range of conditions in the present study. The diagonal stripe pattern approximates a P–T range corresponding to steeply dipping, cold subduction zones. Light gray curves are metamorphic facies boundaries (Spear, 1993); zeo = zeolite, pp = prehnite-pumpellyite, gs = greenschist, bs = blueschist, ext = extraterrestrial.

$$CO_{2(aq)} + 3H_{2(aq)} = CH_3OH_{(aq)} + H_2O_{(l)} \quad (7)$$

Log K_{MOH} isopleths over the P–T range of Fig. 14 show that an isothermal increase in P increases the thermodynamic drive for methanol formation, implying enhanced methanogenesis kinetics. This may be contextualized geologically by considering two hypothetical serpentinization settings at different pressures. The first is a low-P setting at 200 °C and 0.5 kbar (Fig. 14, open star L), conditions similar to those of a previous experimental simulation of seafloor serpentinization in which $[CH_3OH]$ and $[CH_4]$ were correlated (200 °C, 0.3 kbar; Seewald et al., 2006). The second is a high-P setting at 200 °C and 5 kbar (Fig. 14, open star H), representing serpentinized forearc mantle in an old, steeply-dipping subduction zone, e.g., in the Western Pacific (Hyndman and Peacock, 2003; Mottl et al., 2004). Comparison of the log K_{MOH} values for the two locations shows that the thermodynamic drive for methanol formation is substantially greater in the forearc than in the seafloor setting, implying greater methane yields in the former.

Except in cold subduction zones, an increase in lithospheric depth is usually accompanied by an increase in temperature, which could decrease the thermodynamic drive for methanol formation and, consequently, decrease the rate of methanogenesis. Such an effect would apply to any prograde P–T path whose slope is lower than that of the log K_{MOH} isopleths: e.g., an average terrestrial geothermal gradient (gray arrow, Fig. 14). From two to five kilobars along this P–T path, log K_{MOH} decreases by six units, suggesting that methanol-dependent methanogenesis rates would decrease substantially along an average thermal depth profile or, for example, along a prograde path in a warm subduction zone.

Due to the lack of thermodynamic data for Fe-carbonyls over a wide range of geological conditions, it is not possible to model Fe-pentacarbonyl formation in the experimental fluids as a function of P and T. Nevertheless, the results of previous experimental studies suggest that carbonyl formation is favorable over a wide range of lithospheric conditions. Fluid-hosted Fe-carbonyls have been detected in low-grade hydrothermal experiments (250 °C, 0.5–2.0 kbar) in the presence of Fe-sulfides (Cody et al., 2000, 2004), and at higher P and T in diamond anvil cell experiments (250–560 °C, 10–70 kbar) in the presence of a variety of Fe-bearing materials (FeO, Fe°, $FeCO_3$) (Sharma et al., 2009). This P–T range substantially overlaps the stability range of CH_4-rich fluids in the lithosphere (Fig. 1), where Fe-rich minerals such as sulfides and oxides are ubiquitous, implying fluid-hosted carbonyl-mediated methanogenesis is a viable process throughout the crust and upper mantle.

The final mechanism to consider for natural systems is a pressure effect on the rate of catalysis by Fe. Natural gold typically contains trace or minor amounts of Fe on the order of 10^3–10^4 ppm (McInnes et al., 2008), although methanogenesis catalyzed by natural gold is not likely to be a widespread geological process. Metallic Fe is more commonly found in nature as awaruite, wherein the average X_{Fe} value is ~0.3. If heterogeneous catalysis by Fe° is accelerated by pressure, then methanogenesis during awaruite-stabilized serpentinization in the forearc mantle wedge

may be more rapid than during awaruite-stabilized serpentinization at the seafloor. A kinetic pressure effect on heterogeneous catalysis may apply to other proposed FTT catalysts such as sulfides and chromites (Foustoukos and Seyfried, 2004; Fu et al., 2008).

Regardless of the mechanism, the experiments suggest that pressure enhances the kinetics of aqueous methanogenesis along isothermal or very steep P–T paths. The limited experimental pressure range ($\Delta P = 2.5$ kbar) suggests that the pressure differences in nature need not be very large in order for a kinetic effect to be observable: a change in depth of just a kilometer or two along a steep P–T path may be sufficient to significantly increase methane yields. Either methanogenesis in such pressurized fluids is kinetically controlled, in which pressure may play a role, or fluid residence times are sufficiently long that methane equilibrates. In either case, serpentinization of the forearc mantle wedge may be a particularly favorable setting for methanogenesis. Absolute methane concentrations in the serpentinized forearc mantle wedge would also be substantially augmented by pressure-induced increases in mineral solubilities in aqueous fluids at depth. For example, fluids that equilibrate with calcite at blueschist conditions during dehydration of the downgoing slab will contain CO_2 concentrations that are 100–1000X higher than similar fluids in oceanic settings (Caciagli and Manning, 2003), potentially leading to correspondingly high CH_4 yields as these fluids infiltrate and serpentinize the overlying forearc mantle wedge (Lazar et al., 2014). It has been proposed that the progress of H_2- and CH_4-producing reactions in the mantle wedge is limited by Fe-Mg redox partitioning between olivine and the high-pressure serpentine polymorph, antigorite (Evans, 2010), but observations of CH_4-rich, graphite-free fluid inclusions in ultramafic complexes exhumed from mantle wedge settings (Shi et al., 2005; Sachan et al., 2007; Song et al., 2009) demonstrate that extensive aqueous methanogenesis is possible in this environment.

A pressure effect on methanogenesis has astrobiological implications. Because the kinetic barrier to methanogenesis favors the synthesis of metastable organic molecules such as amino acids (Shock, 1990, 1992; Shock and Canovas, 2010), the experimental results imply that prebiotic chemistry may be sensitive to pressure, depending on the local geothermal gradient. Moreover, methane-generating serpentinization has been proposed to be a favorable setting for early Earth and extraterrestrial life (Schulte et al., 2006; Russell et al., 2010), and previous experimental and field studies suggest the viability of a deep biosphere (Gold, 1992; Stevens and McKinley, 1995; Sharma et al., 2002). Therefore, the results imply that microbial habitability for CH_4-dependent organisms varies with pressure. For example, methanogens that exploit slow methanogenesis kinetics may find seafloor serpentinite springs a more favorable habitat than serpentinization at a few kilometers depth in a cool forearc.

5. CONCLUSIONS

Methane generated abiotically in the lithosphere and mantle may have an important influence on the development of a biosphere and atmosphere on Earth and other Solar System bodies. Therefore, understanding the physical chemistry of abiotic methanogenesis is critical in geochemistry, astrobiology, and related disciplines. Because methane-bearing fluids emanating from some submarine springs are not at equilibrium, kinetics may play a role in determining the compositions of such fluids. We examined the effect of pressure on methanogenesis kinetics in four series of cold-seal hydrothermal experiments at 300 °C using a dilute aqueous solution containing $^{13}CO_2$ and H_2 as primary reactants. Experimental methane concentrations did not reach equilibrium and could be explained by two simultaneous effects. The first effect was pressure-independent variations in CH_4 yields between and within the four series of experiments due to heterogeneous catalysis by trace Fe in the Au capsules. The second was a pressure effect attributed to a pressure-dependent increase in the relative concentration of methanol or other reaction intermediate, the stability of Fe-carbonyls, or the rate of heterogeneous catalysis by trace Fe in the Au capsules. The results may aid in modeling methanogenesis in natural settings because pressure may be an important kinetic variable where geologically applicable, e.g., in forearc regions of subduction zones or on planetary seafloors. In geological settings at low T and high P, a pressure effect on methanogenesis kinetics may counteract otherwise slow reaction rates expected at low temperature.

ACKNOWLEDGMENTS

We thank Associate Editor Alfonso Mucci for careful editorial handling, and Cécile Konn, Jennifer Stern, Giora Proskurowski, and several anonymous reviewers whose comments substantially improved this manuscript. We also thank C. Manning, D. Sverjensky, R. Hemley, and D. Foustoukos, and B. Mysen for helpful comments and discussions, and D. Foustoukos for assistance in the cold-seal laboratory at the Geophysical Laboratory. C. Lazar warmly thanks the Geophysical Laboratory and its entire staff for generous financial, scientific, and administrative support during a Carnegie Fellowship, which made this study possible. This work was partly supported by the NASA Astrobiology Institute under NASA Cooperative Agreement NCC2-1056.

REFERENCES

Anderson R. B. (1984) *The Fischer–Tropsch Reaction*. Academic Press, London.

Anderson R., Karn F. and Shultz J. (1964) Kinetics of the Fischer–Tropsch synthesis on iron catalysts. *U.S. Bureau Mines Bull.* **614**, 1–45.

Berndt M. E., Allen D. E. and Seyfried, Jr., W. E. (1996) Reduction of CO_2 during serpentinization of olivine at 300 °C and 500 bar. *Geology* **24**, 351–354.

Bonham L. C. (1978) Solubility of methane in water at elevated-temperatures and pressures. *AAPG Bull. – Am. Assoc. Petrol. Geol.* **62**, 2478–2481.

Brooks K. P., Hu J., Zhu H. and Kee R. J. (2007) Methanation of carbon dioxide by hydrogen reduction using the Sabatier process in microchannel reactors. *Chem. Eng. Sci.* **62**, 1161–1170.

Caciagli N. C. and Manning C. E. (2003) The solubility of calcite in water at 6–16 kbar and 500–800 °C. *Contrib. Miner. Petrol.* **146**, 275–285.

Charlou J. L., Fouquet Y., Bougault H., Donval J. P., Etoubleau J., Jean-Baptiste P., Dapoigny A., Appriou P. and Rona P. A. (1998) Intense CH_4 plumes generated by serpentinization of ultramafic rocks at the intersection of the 15 degrees 20′N fracture zone and the Mid-Atlantic Ridge. *Geochim. Cosmochim. Acta* **62**, 2323–2333.

Charlou J. L., Donval J. P., Douville E., Jean-Baptiste P., Radford-Knoery J., Fouquet Y., Dapoigny A. and Stievenard M. (2000) Compared geochemical signatures and the evolution of Menez Gwen (37 degrees 50′N) and Lucky Strike (37 degrees 17′N) hydrothermal fluids, south of the Azores Triple Junction on the Mid-Atlantic Ridge. *Chem. Geol.* **171**, 49–75.

Charlou J. L., Donval J. P., Fouquet Y., Jean-Baptiste P. and Holm N. (2002) Geochemistry of high H_2 and CH_4 vent fluids issuing from ultramafic rocks at the Rainbow hydrothermal field (36 degrees 14′N, MAR). *Chem. Geol.* **191**, 345–359.

Chen J. Y., Jin L. J., Dong J. P., Zheng H. F. and Liu G. Y. (2008) Methane formation from $CaCO_3$ reduction catalyzed by high pressure. *Chin. Chem. Lett.* **19**, 475–478.

Chou I. M., Eugster H. P., Berens P. and Weare J. H. (1978) Diffusion of hydrogen through platinum membranes at high-pressures and temperatures. *Geochim. Cosmochim. Acta* **42**, 281–288.

Cody G. D., Boctor N. Z., Filley T. R., Hazen R. M., Scott J. H., Sharma A. and Yoder, Jr., H. S. (2000) Primordial carbonylated iron-sulfur compounds and the synthesis of pyruvate. *Science* **289**, 1337–1340.

Cody G. D., Boctor N. Z., Brandes J. A., Filley T. R., Hazen R. M. and Yoder, Jr., H. S. (2004) Assaying the catalytic potential of transition metal sulfides for abiotic carbon fixation. *Geochim. Cosmochim. Acta* **68**, 2185–2196.

Dry M. E. (1981) The Fischer–Tropsch synthesis. In *Catalysis Science and Technology* (eds. J. R. Anderson and M. Boudart). Springer-Verlag, Berlin, pp. 159–255.

Evans B. W. (2010) Lizardite versus antigorite serpentinite: Magnetite, hydrogen, and life(?). *Geology* **38**, 879–882.

Fiebig J., Woodland A. B., Spangenberg J. and Oschmann W. (2007) Natural evidence for rapid abiogenic hydrothermal generation of CH_4. *Geochim. Cosmochim. Acta* **71**, 3028–3039.

Fischer F. and Tropsch H. (1926) The direct synthesis of petroleum hydrocarbons with standard pressure. (First report). *Ber. Dtsch. Chem. Ges.* **59**, 830–831.

Foustoukos D. I. and Seyfried, Jr., W. E. (2004) Hydrocarbons in hydrothermal vent fluids: The role of chromium-bearing catalysts. *Science* **304**, 1002–1005.

French B. M. (1966) Some geological implications of equilibrium between graphite and a C–H–O gas phase at high temperatures and pressures. *Rev. Geophys.* **4**, 223–253.

Frost B. R. (1985) On the stability of sulfides, oxides, and native metals in serpentinite. *J. Petrol.* **26**, 31–63.

Fu Q., Sherwood-Lollar B., Horita J., Lacrampe-Couloume G. and Seyfried, Jr., W. E. (2007) Abiotic formation of hydrocarbons under hydrothermal conditions: Constraints from chemical and isotope data. *Geochim. Cosmochim. Acta* **71**, 1982–1998.

Fu Q., Foustoukos D. I. and Seyfried, Jr., W. E. (2008) Mineral catalyzed organic synthesis in hydrothermal systems: An experimental study using time-of-flight secondary ion mass spectrometry. *Geophys. Res. Lett.* **35**, L07612.

Gold T. (1992) The deep, hot biosphere. *Proc. Natl. Acad. Sci.* **89**, 6045–6049.

Holland T. and Powell R. (1991) A Compensated Redlich–Kwong (CORK) equation for volumes and fugacities of CO_2 and H_2O in the range 1-bar to 50-kbar and 100–1600-degrees-C. *Contrib. Miner. Petrol.* **109**, 265–273.

Horita J. and Berndt M. E. (1999) Abiogenic methane formation and isotopic fractionation under hydrothermal conditions. *Science* **285**, 1055–1057.

Hyndman R. D. and Peacock S. M. (2003) Serpentinization of the forearc mantle. *Earth Planet. Sci. Lett.* **212**, 417–432.

Ingmanson D. E. and Dowler M. J. (1977) Chemical evolution and the evolution of Earth's crust. *Origins of life* **8**, 221–224.

Janecky D. R. and Seyfried, Jr., W. E. (1986) Hydrothermal serpentinization of peridotite within the oceanic crust: Experimental investigations of mineralogy and major element chemistry. *Geochim. Cosmochim. Acta* **50**, 1357–1378.

Jenner G. (2002) Comparative activation modes in organic synthesis. The specific role of high pressure. *Tetrahedron* **58**, 5185–5202.

Ji F., Zhou H. and Yang Q. (2008) The abiotic formation of hydrocarbons from dissolved CO_2 under hydrothermal conditions with cobalt-bearing magnetite. *Orig. Life Evol. Biospheres* **38**, 117–125.

Johnson J. W., Oelkers E. H. and Helgeson H. C. (1992) SUPCRT92 – A software package for calculating the standard molal thermodynamic properties of minerals, gases, aqueous species, and reactions from 1-bar to 5000-bar and 0-degrees-C to 1000-degrees-C. *Comput. Geosci.* **18**, 899–947.

Kasting J. (2005) Methane and climate during the Precambrian era. *Precambr. Res.* **137**, 119–129.

Kelley D. S. (1996) Methane-rich fluids in the oceanic crust. *J. Geophys. Res.-Solid Earth* **101**, 2943–2962.

Kelley D. S., Karson J. A., Fruh-Green G. L., Yoerger D. R., Shank T. M., Butterfield D. A., Hayes J. M., Schrenk M. O., Olson E. J., Proskurowski G., Jakuba M., Bradley A., Larson B., Ludwig K., Glickson D., Buckman K., Bradley A. S., Brazelton W. J., Roe K., Elend M. J., Delacour A., Bernasconi S. M., Lilley M. D., Baross J. A., Summons R. E. and Sylva S. P. (2005) A serpentinite-hosted ecosystem: The Lost City hydrothermal field. *Science* **307**, 1428–1434.

Kenney J. F., Kutcherov V. A., Bendeliani N. A. and Alekseev V. A. (2002) The evolution of multicomponent systems at high pressures: VI. The thermodynamic stability of the hydrogen-carbon system: The genesis of hydrocarbons and the origin of petroleum. *Proc. Natl. Acad. Sci.* **99**, 10976–10981.

Klein F. and Bach W. G. (2009) Fe–Ni–Co–O–S phase relations in peridotite–seawater interactions. *J. Petrol.* **50**, 37–59.

Kolesnikov A., Kutcherov V. G. and Goncharov A. F. (2009) Methane-derived hydrocarbons produced under upper-mantle conditions. *Nat. Geosci.* **2**, 566–570.

Lazar C., McCollom T. M. and Manning C. E. (2012) Abiogenic methanogenesis during experimental komatiite serpentinization: Implications for the evolution of the early Precambrian atmosphere. *Chem. Geol.* **326–327**, 102–112.

Lazar C., Zhang C., Manning C. E. and Mysen B. O. (2014) Redox effects on calcite-portlandite-fluid equilibria at forearc conditions: Carbon mobility, methanogenesis, and reduction melting of calcite. *Am. Mineral.* **99**, 1604–1615.

Lewis G. N. and Randall M. (1923) *Thermodynamics*. McGraw Hill, New York.

Li Z. X. A. and Lee C. T. A. (2006) Geochemical investigation of serpentinized oceanic lithospheric mantle in the Feather River Ophiolite, California: Implications for the recycling rate of water by subduction. *Chem. Geol.* **235**, 161–185.

Lyons J. R., Manning C. and Nimmo F. (2005) Formation of methane on Mars by fluid–rock interaction in the crust. *Geophys. Res. Lett.* **32**, L13201.

McCollom T. M. (2013) Laboratory simulations of abiotic hydrocarbon formation in Earth's deep subsurface. *Rev. Mineral. Geochem.* **75**, 467–494.

McCollom T. M. and Seewald J. S. (2001) A reassessment of the potential for reduction of dissolved CO_2 to hydrocarbons during serpentinization of olivine. *Geochim. Cosmochim. Acta* **65**, 3769–3778.

McCollom T. M. and Seewald J. S. (2003) Experimental constraints on the hydrothermal reactivity of organic acids and acid anions: I. Formic acid and formate. *Geochim. Cosmochim. Acta* **67**, 3625–3644.

McCollom T. M. and Seewald J. S. (2006) Carbon isotope composition of organic compounds produced by abiotic synthesis under hydrothermal conditions. *Earth Planet. Sci. Lett.* **243**, 74–84.

McCollom T. M. and Seewald J. S. (2007) Abiotic synthesis of organic compounds in deep-sea hydrothermal environments. *Chem. Rev.* **107**, 382–401.

McCollom T. M., Sherwood-Lollar B. S., Lacrampe-Couloume G. and Seewald J. S. (2010) The influence of carbon source on abiotic organic synthesis and carbon isotope fractionation under hydrothermal conditions. *Geochim. Cosmochim. Acta* **74**, 2717–2740.

McInnes M., Greenough J. D., Fryer B. J. and Wells R. (2008) Trace elements in native gold by solution ICP-MS and their use in mineral exploration: A British Columbia example. *Appl. Geochem.* **23**, 1076–1085.

Miller S. L. and Urey H. C. (1959) Organic compound synthesis on the primitive Earth. *Science* **130**, 245–251.

Mori Y., Nishiyama T. and Yanagi T. (2003) Mass transfer and reaction paths in alteration zones around carbonate veins in the Nishisonogi Metamorphic Rocks, southwest Japan. *Am. Mineral.* **88**, 611–623.

Mottl M. J., Komor S. C., Fryer P. and Moyer C. L. (2003) Deep-slab fuel extremophilic Archaea on a Mariana forearc serpentinite mud volcano: Ocean Drilling Program Leg 195. *Geochem. Geophys. Geosyst.* **4**(11), 9009. http://dx.doi.org/10.1029/2003GC000588.

Mottl M. J., Wheat C. G., Fryer P., Gharib J. and Martin J. B. (2004) Chemistry of springs across the Mariana forearc shows progressive devolatilization of the subducting plate. *Geochim. Cosmochim. Acta* **68**, 4915–4933.

Peretti A., Dubessy J., Mullis J., Frost B. R. and Trommsdorff V. (1992) Highly reducing conditions during Alpine metamorphism of the Malenco Peridotite (Sondrio, Northern Italy) indicated by mineral paragenesis and H-2 in fluid inclusions. *Contrib. Miner. Petrol.* **112**, 329–340.

Potter J., Rankin A. H., Treloar P. J., Nivin V. A., Ting W. P. and Ni P. (1998) A preliminary study of methane inclusions in alkaline igneous rocks of the Kola igneous province, Russia: Implications for the origin of methane in igneous rocks. *Eur. J. Mineral.* **10**, 1167–1180.

Potter J., Rankin A. H. and Treloar P. J. (2004) Abiogenic Fischer–Tropsch synthesis of hydrocarbons in alkaline igneous rocks; fluid inclusion, textural and isotopic evidence from the Lovozero complex, N.W. Russia. *Lithos* **75**, 311–330.

Proskurowski G., Lilley M. D., Seewald J. S., Fruh-Green G. L., Olson E. J., Lupton J. E., Sylva S. P. and Kelley D. S. (2008) Abiogenic hydrocarbon production at Lost City hydrothermal field. *Science* **319**, 604–607.

Roferdepoorter C. K. (1981) A comprehensive mechanism for the Fischer–Tropsch synthesis. *Chem. Rev.* **81**, 447–474.

Russell M. J., Hall A. J. and Martin W. (2010) Serpentinization as a source of energy at the origin of life. *Geobiology* **8**, 355–371.

Sabatier P. and Gaudion G. (1919) Catalytic dehydrogenation by nickel in the presence of hydrogen. *Comptes Rendus Hebdomadaires Des Seances De L'Academie Des Sciences* **168**, 670–672.

Sachan H. K., Mukherjee B. K. and Bodnar R. J. (2007) Preservation of methane generated during serpentinization of upper mantle rocks: Evidence from fluid inclusions in the Nidar ophiolite, Indus Suture Zone, Ladakh (India). *Earth Planet. Sci. Lett.* **257**, 47–59.

Schulte M., Blake D., Hoehler T. and McCollom T. M. (2006) Serpentinization and its implications for life on the early Earth and Mars. *Astrobiology* **6**, 364–376.

Scott H. P., Hemley R. J., Mao H. K., Herschbach D. R., Fried L. E., Howard W. M. and Bastea S. (2004) Generation of methane in the Earth's mantle: In situ high pressure–temperature measurements of carbonate reduction. *Proc. Natl. Acad. Sci.* **101**, 14023–14026.

Seewald J. S., Zolotov M. Y. and McCollom T. M. (2006) Experimental investigation of single carbon compounds under hydrothermal conditions. *Geochim. Cosmochim. Acta* **70**, 446–460.

Seward T. M. and Franck E. U. (1981) The system hydrogen-water up to 440 degrees C and 2500 bar pressure. *Ber. Bunsenges. Phys. Chem* **85**, 2–7.

Seyfried, Jr., W. E., Janecky D. R. and Berndt M. E. (1987) Rocking autoclaves for hydrothermal experiments, II. The flexible reaction-cell system. In *Hydrothermal Experimental Techniques* (eds. G. C. Ulmer and H. L. Barnes). John Wiley and Sons, pp. 216–239.

Sharma A., Scott J. H., Cody G. D., Fogel M. L., Hazen R. M., Hemley R. J. and Huntress W. T. (2002) Microbial activity at gigapascal pressures. *Science* **295**, 1514–1516.

Sharma A., Cody G. D. and Hemley R. J. (2009) In situ diamond-anvil cell observations of methanogenesis at high pressures and temperatures. *Energy Fuels* **23**, 5571–5579.

Sherwood-Lollar B., Westgate T. D., Ward J. A., Slater G. F. and Lacrampe-Couloume G. (2002) Abiogenic formation of alkanes in the Earth's crust as a minor source for global hydrocarbon reservoirs. *Nature* **416**, 522–524.

Shi G. U., Tropper P., Cui W. Y., Tan J. and Wang C. Q. (2005) Methane (CH_4)-bearing fluid inclusions in the Myanmar jadeitite. *Geochem. J.* **39**, 503–516.

Shock E. L. (1988) Organic acid metastability in sedimentary basins. *Geology* **16**, 886–890.

Shock E. L. (1990) Geochemical constraints on the origin of organic compounds in hydrothermal systems. *Orig. Life Evol. Biosph.* **20**, 331–367.

Shock E. L. (1992) Chemical environments of submarine hydrothermal systems. *Orig. Life Evol. Biosph.* **22**, 67–107.

Shock E. L. and Canovas P. (2010) The potential for abiotic organic synthesis and biosynthesis at seafloor hydrothermal systems. *Geofluids* **10**, 161–192.

Shuai Y., Peng P. and Zou Y. (2006) Influence of pressure on stable carbon isotope ratio and production yield of coal-derived methane. *Fuel* **85**, 860–866.

Spear F. S. (1993) Metamorphic phase equilibria and pressure-temperature-time paths. *Mineral. Soc. Am. Monogr.* **1**, 793.

Song S. G., Su L., Niu Y. L., Lai Y. and Zhang L. F. (2009) CH_4 inclusions in orogenic harzburgite: Evidence for reduced slab fluids and implication for redox melting in mantle wedge. *Geochim. Cosmochim. Acta* **73**, 1737–1754.

Stevens T. O. and McKinley J. P. (1995) Lithoautotrophic microbial ecosystems in deep basalt aquifers. *Science* **270**, 450–455.

Tao W., Zou Y., Carr A., Liu J. and Peng P. (2010) Study of the influence of pressure on enhanced gaseous hydrocarbon yield under high pressure–high temperature coal pyrolysis. *Fuel* **89**, 3590–3597.

Tuttle O. F. (1949) Two pressure vessels for silicate-water studies. *GSA Bull.* **60**, 1727–1729.

Vance S., Harnmeijer J., Kimura J., Hussmann H., Demartin B. and Brown J. M. (2007) Hydrothermal systems in small ocean planets. *Astrobiology* **7**, 987–1005.

Yu J. L. and Savage P. E. (1998) Decomposition of formic acid under hydrothermal conditions. *Ind. Eng. Chem. Res.* **37**, 2–10.

Associate editor: Alfonso Mucci